Biogeosciences Discuss., 6, 9817–9848, 2009
www.biogeosciences-discuss.net/6/9817/2009/

Biogeosciences Discussions

Biogeosciences Discussions is the access reviewed discussion forum of *Biogeosciences*

Effect of CO_2 on the properties and sinking velocity of aggregates of the coccolithophore *Emiliania huxleyi*

A. Biermann[1,*] **and A. Engel**[1]

[1]Alfred Wegener Institute for Polar and Marine Research, Am Handelshafen 12, 27570 Bremerhaven, Germany
[*]now at: IFM-GEOMAR, Leibniz Institute of Marine Sciences, Düsternbrooker Weg 20, 24105 Kiel, Germany

Received: 8 September 2009 – Accepted: 23 September 2009 – Published: 13 October 2009

Correspondence to: A. Biermann (abiermann@ifm-geomar.de)

Published by Copernicus Publications on behalf of the European Geosciences Union.

Abstract

Coccolithophores play an important role in organic matter export due to their production of the mineral calcite that can act as ballast. Recent studies indicated that calcification in coccolithophores may be affected by changes in seawater carbonate chemistry. We investigated the influence of CO_2 on the aggregation and sinking behaviour of the coccolithophore *Emiliania huxleyi* (PML B92/11) during a laboratory experiment. The coccolithophores were grown under low (~180 µatm), medium (~380 µatm), and high (~750 µatm) CO_2 conditions. Aggregation of the cells was promoted using roller tables. Size and settling velocity of aggregates were determined during the incubation using video image analysis. The results show that CO_2 induced changes in the inorganic carbon to organic carbon ratio (PIC/POC) influence the porosity and hence the sinking velocity of aggregates of *Emiliania huxleyi*. Average sinking velocity was highest for low CO_2 aggregates (~1292 m d^{-1}) that also had the highest PIC/POC ratio. Lowest PIC/POC ratios and lowest sinking velocity (~366 m d^{-1}) at comparable sizes were observed for aggregates of the high CO_2 treatment. Aggregates of the high CO_2 treatment showed an excess density about one order of magnitude lower (~4.2×10^{-4} g cm^{-3}) when compared to aggregates from the medium and low CO_2 treatments (~1.7×10^{-3} g cm^{-3}). Thus, the amount of calcite in aggregates is crucial for the degree of ballasting effect. In the high CO_2 treatment, aggregates with lower calcite content had higher bacterial abundance, suggesting enhanced bacterial degradation. Thus, our findings indicate that a CO_2 induced reduction of calcite content aggregates could affect the vertical export of organic matter in the ocean, particularly in areas dominated by coccolithophores blooms.

1 Introduction

In times of rising atmospheric CO_2, the marine carbon cycle gains more and more attention for several reasons. The ocean is the largest sink for atmospheric CO_2 (Sabine

BGD

6, 9817–9848, 2009

et al., 2004) due to the physical uptake of CO_2, the chemical conversion of CO_2 into bicarbonate and carbonate, and the sequestration of carbon into deeper layers of the ocean via the biological pump. A small fraction of exported carbon is deposited in the worlds' oceans sediments where it is partly conserved on a time scale of years to centuries.

The major fraction of organic matter is transported to the ocean's interior by aggregates, in form of marine snow or fecal pellets (Honjo, 1982; Fowler and Knauer, 1986). Lithogenic or terrestrial material of eolian or riverine origin can act as ballast since it increases the density of organic matter (Ittekot and Haake, 1990). Recent findings suggest that the flux of organic matter at depth ~1800 m is directly proportional to the fluxes of ballast minerals (Armstrong et al., 2002; Francois et al., 2002; Klaas and Archer, 2002). Thereby, the mineral phase may protect from degradation, or the organic matter may serve as glue that binds particles together and aggregates may disintegrate if the particulate organic carbon (POC) content becomes too low (Armstrong et al., 2002). A comparison of sediment trap data below 1000 m from 52 locations around the world confirmed that most of the organic carbon that is transferred to the deep sea is carried by calcium carbonate (Klaas and Archer, 2002).

Coccolithophores are major calcifying organisms and highly abundant in temperate and sub-polar regions of the oceans and are well known to develop large blooms with densities of up to several 10^5 cells ml^{-1} seawater (Holligan et al., 1983; Robertson et al., 1991; van der Wal et al., 1995; Kleypas, 2006; Raitos et al., 2006). Coccolithophores precipitate a sphere of calcium carbonate (calcite) platelets, the coccoliths (Paasche, 2002; Kleypas, 2006; Langer et al., 2006). In experimental studies with the coccolithophore *E. huxleyi*, increased CO_2 concentrations led to lower rates of calcite precipitation when compared to organic matter production (Riebesell et al., 2000; Zondervan et al., 2001, 2002). However, other studies revealed either an opposite effect of elevated CO_2 concentrations on coccolithophores (Iglesias-Rodriguez et al., 2008) or suggest a strain-specific response of *E. huxleyi* under increased CO_2 levels (Langer et al., 2009). A study with calcifying and non-calcifiying coccolithophores revealed that

calcite has a strong effect on coccolithophores aggregate properties, leading to higher excess density and settling velocity of calcareous aggregates (Engel et al., 2009b). It was also demonstrated that aggregates without coccoliths were more prone to decomposition (Engel et al., 2009a).

Here, we investigate how different CO_2 concentrations during an *E. huxleyi* bloom may affect the formation and calcite ballasting of aggregates.

We hypothesized that an increase in CO_2 concentration leads to enhanced organic carbon production in coccolithophores due to a stimulation of photosynthetic rates as shown by Rost et al. (2003). At the same time, CO_2 induced acidification of seawater can also affect calcification of cells, reducing weight and with it the "ballast" of cells. CO_2 induced changes in organic carbon content and in the degree of mineral ballast could thus affect the recycling and sinking rates of aggregates of coccolithophores, with potentially important implications for organic matter export in the future ocean.

2 Methods

2.1 Experimental setup

The calcifying strain *Emiliania huxleyi* (PML B92/11) was grown in 20-L bottles at three different CO_2 conditions for 13 days. Adjustment of the pCO_2 was achieved by an aeration system: In order to simulate the low CO_2 treatment (LCT) of ~180 µatm and the high CO_2 treatment (HCT) of ~750 µatm, pure CO_2 was mixed with CO_2-free air. For the medium CO_2 treatment (MCT) of ~380 µatm CO_2, ambient air was used. For control and adjustment of CO_2 concentration, a LICOR Li-6252 gas analyzer was used. For reassuring a well mixing the cultures were bubbled at the bottom of the bottles. The cells were grown in 0.2 µm filtrated North Sea water with a salinity of 32.3 (Cond 330i, WTW) at a temperature of 17±0.2°C. The water was enriched with nutrients to yield 155 µmol L^{-1} $NaNO_3$ and 11 µmol L^{-1} Na_2HPO_4 initially. In addition, trace nutrients were added according to the *F*/2 recipe of Guillard and Ryther (1962). The

day to night cycle was adjusted to 16:8 h with a light intensity during day hours of 218±10 µmol photons m^{-2} s^{-1}. Prior to the experiment, all tubes and bottles were either autoclaved or washed with 10% HCl, and rinsed thoroughly with MilliQ water.

Because aggregate formation has most often been observed towards the end of phytoplankton blooms, the aggregation experiment was started after 7 days of the stationary growth (T14; Table 1). Therefore, the cultures were transferred into a total of nine transparent, cylindrical tanks.

For each treatment one 10-L tank and two 4.5-L tanks were filled and immediately put onto roller tables. The roller table experiments started at a cell abundance of 2.6×10^6 cells ml^{-1} for LCT, 2.2×10^6 cells ml^{-1} for the MCT and 2.5×10^6 cells ml^{-1} for the HCT. Although natural blooms achieve lower cell densities of up to 3.5×10^5 cells ml^{-1} (Robertson et al., 1991), we chose higher abundances to assure that enough cell material was present for aggregate formation. The rotation speed was set to 2.35±0.05 rpm. During the experiment, the rotation speed of tanks was repeatedly increased in order to prevent the aggregates from colliding with the tank walls (Engel et al., 2009b).

The pH in the tanks was determined during the roller table experiment in one of the 4.5-L tanks of each treatment at T_{18}, yielding values of 8.9, 7.9 and 7.6 for the LCT, MCT and HCT, respectively.

The 10-L tanks were used for recording aggregates with a video camera. Video pictures were analyszed using image analysis and sinking velocity and other aggregate properties were determined after Engel and Schartau (1999). Aggregates were filmed each day twice for 10 min with a digital camera (Sony digital 8 DCR-TRV460) equipped with an 80-mm macro lens. The distance between the 4 cm×5 cm observation area (x/y coordination grid) and the lens was 5 cm. The observation area was chosen on the right side in the middle of the horizontal axis, since the tank was rotating anticlockwise and aggregates accumulated in this area (Tooby et al., 1977). Additionally, a mm-scale was put onto the tank at the observation area for determining the aggregates sizes. The videos were recorded to a PC with the software Pinnacle Studio Plus

700-PCI, and single pictures were analysed using ImageJ 1.38 (Wayne Rasband, National Institutes of Health, Bethesda, Maryland, USA). Aggregates were marked and the following parameters determined: their position (x, y), area, length of the longest axis (major), length of the shortest axis (minor) and x-feret diameter (d_f), which is the largest size of an aggregate in the horizontal direction. The number of analyzed aggregates was n=71 for the LCT, and n=63 and n=65 for the MCT and HCT, respectively.

For the dimensionless drag coefficient (Cd) we assumed a value of $95(\mathrm{Re})^{-1.85}$ after Alldredge and Gotschalk (1988) and $\mathrm{Re}=dU/\nu$, where d is the particle diameter, U is the sinking velocity of the particle, and ν the kinematic viscosity of the fluid. The kinematic viscosity of the fluid is the quotient of dynamic viscosity (ζ) and the density of the fluid (ρ_{fl}). The dynamic viscosity (ζ) was 0.0118 $\mathrm{cm^2\,s^{-1}}$, interpolated according to Dietrich et al. (1975) for a temperature of 17°C and salinity of 32.3. The calculated kinematic viscosity was 0.01153 $\mathrm{cm^2\,s^{-1}}$.

2.2 Sampling

On four days samples were taken for the analyses of bacteria, nutrients, scanning electron microscopy (SEM), total alkalinity (TA), total particulate carbon (TPC), particulate organic and inorganic carbon (POC and PIC), particulate organic nitrogen (PON), dry weight (DW), cell counts and total particle volume (TPV), and pH (see Table 1 for a more detailed description).

On the last day of the experiment (T21), all tanks were removed carefully from the rolling tables and turned to one side. About 15 min after, the aggregates had settled to the bottom and were isolated from the surrounding cell suspension using a 10 ml serological pipette. From each tank, all visible aggregates (>1 mm) were collected, pooled and the total amount of aggregate slurry determined. Afterwards, the slurry was diluted with one litre of NaCl solution, adjusted to sample salinity. Samples were also taken from the surrounding cell suspension (SUSP) containing no visible aggregates. To determine the total amount of particulate matter within the aggregate fraction (AGG), the amount of particulate constituents determined for the slurry (SL) was corrected for

particulate material by-harvested from SUSP according to:

$$(x)_{AGG} = (V_{SL} \cdot cx_{SL}) - (V_{SL} \cdot cx_{SUSP}) \quad (1)$$

where V_{SL} is the volume of the slurry, cx_{SL} is the concentration of a parameter x of the slurry, cx_{SUSP} is the concentration of a component x of the background suspension (Engel et al., 2002).

2.3 Chemical analyses, cell counts, TPV and SEM

For the determination of nutrients 50 ml of sample were 0.2 µm filtered (Minisart) and stored at −20°C until photometrical processing using an auto analyser (Evolution 3, Alliance Instruments). Determination was performed in duplicate after the method of Grashoff et al. (1999). The detection limit for NO_3^- was 0.3 µmol L^{-1} and for PO_4^{3-} 0.1 µmol L^{-1}. Cell abundance in the size range 2.751–5.789 µm equivalent spherical diameter (ESD) and volume were determined with a coulter counter (Multisizer 3, Beckman). A volume of 0.2–4 ml of samples diluted with 16–20 ml of 0.2 µm filtered seawater was measured in triplicate. Sample dilution was necessary in order to keep the coincidence of particles at the 100 µm aperture <5%. The total particle volume (TPV) was determined as the sum of volumes of individual particles. The pH and temperature was determined with a WTW pH meter (model 340 i) at day T0, T6, T14 and T21. Alkalinity was determined at days T0, T6, T14, and T21 from 200 ml sample filtrated through precombusted (8 h at 500°C) GF/F filters (Whatman). The samples were stored in the dark at 0°C until analysis by potentiometric titration (Brewer et al. 1986), using a Metrohm 665 dosimeter and a 713 pH-meter. Total alkalinity was calculated from Gran plots (Gran, 1952). The calcite saturation state (Ω) was calculated with the help of pH and TA, using the software CO2SYS (Lewis and Wallace, 1998). DW of particulate matter was determined from 10–100 ml of sample taken at T0, T6, T14, and T21 and gently (<200 mbar) filtered onto pre-weighed and combusted (8 h, 500°C) GF/F filters (Whatman). The filters were oven dried for 24 h at 60°C and reweighed. For TPC, POC, and PON, 10–100 ml sample was filtered onto precombusted (8 h, 500°C)

GF/F filters (Whatman) and measured on an elemental analyzer (model Euro EA). Before elemental analysis, filters were dried for 24 h at 60°C. For POC, one set of filters was acidified with 5 to 8 drops of 0.1 N HCl in order to remove inorganic carbon. PIC was then calculated by subtracting POC from TPC. Filters for dry weight, TPC, PON, POC, and PIC were stored at −20°C until analysis. At T0 and T6 only single filters were prepared for each treatment, whereas triplicates for SUSP and AGG were obtained at T14 and T21.

For bacterial abundance, 5 ml of both SUSP and aggregate slurry were collected in duplicate at T14 and in triplicate at T21 (Table 1), preserved with GDA to an end concentration of 0.023%, and frozen at −20°C until measurement. Bacterial abundance was determined with a Becton Dickinson Facscalibur flow cytometer and using CellQuest 3.3 (Becton Dickinson) and WinMD 2.8 (J. Trotter, The Scripps Institute, La Jolla, CA). The flow cytometer was equipped with an air cooled argon laser (15 mW, Ex. 488 nm). Fluorescence (FL1) was detected with a standard filter set-up (Em. 530 ±15 nm) and analyses performed at the lowest flow rate (approx. 14 µl min^{-1}). Event range was between 200 and 800 s^{-1}. Prior to measurement, 20 µl of sample was diluted with deionised water to a concentration of 10%. Bacteria then were stained with 5 µl of the fluorescence dye SybrGreen I (Invitrogen) diluted in DMSO to an end concentration of 2.5%. 5 µl fluorescent beads (Polyscience) were used for the internal volume normalization and calibrated against Trucount beads (Becton Dickinson) for absolute volume concentration calculation. After the visual inspection of the dot plots of FL 1 and side scatter (SSC) a manual gating was performed (Gasol and Giorgio, 2000).

An overview of the results of chemical analyses of suspensions before transfer to the roller tanks (T14) is given in Table 2.

For scanning electron microscopy (SEM), 5 to 15 ml of sample were filtered (<200 mbar) onto 0.2 µm polycarbonate filters (Sartorius), dried, and sputtered with gold-palladium. Analysis was made with a Qanta 200 F (Fei) electron microscope. For each CO_2 treatment and sampling day 5 to 12 pictures were made and analysed

qualitatively within a magnification range of 1000× to 40 000×.

2.4 Statistics

Nonlinear curve fits were performed with SigmaPlot 10.0. (SysStat). The treatments were compared by analysis of variance (ANOVA), significant differences calculated with Tukey's HSD test, and homogeneity of variances checked with Levene's test (Statistica 8.0, StatSoft). Additionally, Kruskal-Wallis tests were performed for not normal distributed data. Statistical significance was accepted for $p<0.05$.

3 Results

3.1 Aggregate properties derived from video picture analysis

3.1.1 Aggregate shape, size and sinking velocity

Visible aggregates appeared within 12 h in all roller tanks. The shape of aggregates clearly differed between the CO_2 treatments (pictures not shown). While aggregates that formed in the LCT were compact and spherical, aggregates of the HCT treatment seemed to be more fragile, fluffy and elongated. Aggregates of the MCT took in an intermediate position, being not as compact as the LCT aggregates but also spherical.

Figure 1a shows the size of aggregates for the different treatments, displayed as the equivalent spherical diameter (ESD) of an aggregate. The largest aggregates were observed in the HCT, with an average size of 0.367 cm±0.090 and with a maximum size of 0.669 cm. Aggregates of the LCT were significantly smaller than in the HCT ($p<0.001$), reaching on average 0.268±0.085 cm and a maximum size of 0.565 cm. The smallest aggregates, however, were those of the MCT with on average 0.230±0.061 cm (MCT vs. LCT: $p<0.05$, MCT vs. HCT $p<0.001$). In addition, the variability of aggregate sizes was smallest for the MCT.

The sinking velocity of aggregates differed significantly ($p<0.001$) between the CO_2 treatments (Fig. 1b). Although the aggregates of the HCT were largest, their sinking velocity was the lowest of all CO_2 treatments. Sinking velocity of HCT aggregates was on average 0.4 cm s^{-1} or 366 m d^{-1}. MCT aggregates were sinking with an average rate of 0.9 cm s^{-1} or 740 m d^{-1}. Sinking speed of LCT aggregates was the fasted with on average 1.5 cm s^{-1}, 1292 m d^{-1}, respectively.

A non-linear relationship between aggregate size (x, cm) and sinking velocity (y, cm s^{-1}) was determined only for aggregates of the LCT, yielding $y=3.75x^{0.7}$ ($r^2=0.58$). For MCT- and HCT aggregates, size and sinking velocity were not correlated (Fig. 2).

3.1.2 Porosity, excess density, and mass of aggregates

The porosity (P) of an aggregate was calculated according to (Engel and Schartau, 1999):

$$P = 1 - (\Delta p / p_p) \quad (2)$$

For the density of the particle (p_p), we assumed 1.19 g cm^{-3} for fully calcified cells of the LCT aggregates (Fig. 5a), according to Paasche (2002). For the less calcified and naked cells of MCT and HCT (Fig. 5b), we calculated the porosity with a density of 1.095 g cm^{-3}, as determined for non-calcified cells by Engel et al. (2009b).

The porosity of HCT aggregates was on average 99.96±0.03%, and significantly higher ($p<0.001$) than porosities of MCT- and LCT aggregates, which were quite similar with 99.85±0.09% and 99.86±0.2%, respectively (Fig. 1c).

The excess density (Δp) of an aggregate was derived from settling velocity (Engel and Schartau, 1999).

The Δp of HCT aggregates were significantly different from those of MCT and LCT aggregates ($p<0.001$) (Fig. 1d). The Δp for HCT was on average $4.2\times10^{-4}\pm3.4\times10^{-4}$ g cm^{-3} and one order of magnitude smaller than the Δp of MCT and LCT aggregates. Aggregates of the MCT had an average Δp of

$1.7\times10^{-3}\pm1.1\times10^{-3}$ g cm^{-3} and differed hardly from LCT aggregates with an average Δp of $1.7\times10^{-3}\pm2.4\times10^{-3}$ g cm^{-3}. Figure 3 shows a general decrease in Δp with size of aggregates in the three treatments. This figure illustrates that LCT aggregates had higher excess densities even at large sizes, compared to the low excess densities of large HCT aggregates. The MCT aggregates took in an intermediate position between LCT and HCT aggregates.

The mass of an aggregate was calculated from Δp multiplied with the aggregate volume (V_{ag}) as derived from the video picture analysis:

$$\text{Mass} = \Delta p \times V_{ag} \,. \quad (3)$$

Note, for a better distinction we use the term "mass" for data that was derived from the video picture analysis, whereas the term "dry weight (DW)" of an aggregate is used for the chemical analysis.

The mass (µg) of LCT aggregates was related to the equivalent spherical diameter (ESD, cm) in the power function $y=13.6x^{0.28}$ ($r^2=0.79$) (Fig. 4). The relationship between mass and size was less pronounced for MCT aggregates with $y=11.6x^{0.22}$ ($r^2=0.37$). For HCT aggregates no significant relationship between mass and size was determined.

3.2 Aggregate composition

3.2.1 Aggregate volume

The total amount of aggregate fraction that was isolated from the tanks, increased with increasing CO_2 concentration (Table 3). It was ~1.5 times higher for the MCT and ~2.5 times higher for the HCT compared to the LCT. This may partially be explained by increasing porosity and fragility of aggregates in MCT and HCT, leading to a higher amount of background suspension simultaneously harvested with the aggregates. To identify the total particulate volume attributed to aggregates solely (TPV), the cumulative volume of cells and particles within the aggregate fraction (AGG) was determined

with the Coulter Multisizer. TPV was 2-fold higher in the HCT than in MCT, and almost 4-fold higher than in LCT (Table 4), indicating that amount of particles subjected to aggregation increased with increasing CO_2.

3.2.2 Biogeochemistry of aggregates and bacterial abundance

Although TPV was highest in HCT, its total DW of 38.2 mg L^{-1} was almost the same as for the aggregate fractions of the other two treatments with 39.9 and 37.4 mg L^{-1} for LCT and MCT, respectively (Table 4). As a consequence, the ratio of DW to TPV was higher for aggregates in LCT (6.69), compared to MCT (3.09) and HCT (1.81). This can be explained by a higher contribution of PIC, since the density of $CaCO_3$ is ~2.7 g cm^{-3} and hence higher than the average density of organic components (density of cytoplasm: 1.03–1.34 Smayda, 1970). Accordingly, the PIC/POC ratio of aggregates in HCT was only 0.023, and therewith about 5 times smaller than in LCT aggregates (PIC/POC=0.127). Again, PIC/POC for MCT aggregates was intermediate between LCT and HCT, yielding a 3 times higher ratio than for HCT. By relating PIC to TPV, the density fraction of PIC within aggregates was calculated, yielding 0.026 mg mm^{-3} for LCT and 4 times lower values for HCT (0.007 mg mm^{-3}). The density fraction of POC on the other side was on average 1.5-fold higher for MCT and HCT, compared to LCT (0.209 mg mm^{-3}). The contribution of POC to TPC was about 89% for LCT aggregates, 96% for MCT, and almost 100% for HCT aggregates.

Overall, these ratios clearly demonstrated that the POC fraction in aggregates increased when going from LCT to HCT, while the PIC fraction decreased. Comparing the chemical composition of aggregates with the initial cell suspension (Table 2) showed that the POC content was already higher in MCT and HCT than in LCT before the onset of the roller table experiment. The PIC/POC ratio of the cell suspensions yielded on average 0.6 for LCT, and 0.4 and 0.3 for MCT and HCT, respectively (Table 2), suggesting that the differences in aggregate composition were related to the different growth conditions for *E. huxleyi* rather than to differential aggregation of PIC and POC. The ratio of POC/PON was twice as high for cell suspension and aggregates

in MCT and HCT compared to LCT (Tables 2 and 4).

We also calculated enrichment factors (f) to describe the selective enrichment of a component in aggregates compared to the background suspension. The results show only small differences between the CO_2 treatments, except for the PIC density fraction, i.e. the ratio of PIC to TPV. Here, f_{PIC} was lowest for HCT aggregates compared to MCT and LCT (Table 4), suggesting either a lower aggregation rate of PIC in this treatment or PIC dissolution within aggregates. Absolute abundance of bacteria was 2-fold higher in HCT than in LCT aggregates, yielding 5.5×10^8 L ($p<0.05$ ANOVA and K.W.-Test) (Table 4).

At the end of the roller table experiment (T21), values for $\Omega_{calcite}$ had dropped to 4.8 for LCT, 1.8 for MCT and 1.4 for HCT, due to bacterial respiration in the tanks. Significant dissolution of calcite during the incubation was unlikely, since Ω always stayed above 1, but cannot be fully excluded for microzones within the aggregates.

3.2.3 Scanning electron microscopy (SEM)

Figure 5a shows a typical *E. huxleyi* cell observed in all treatments during the growth phase from T0 to T6. At the sampling date T14 "naked" cells – cells without coccoliths, appeared for the first time in all treatments (Fig. 5b). However, in the LCT well formed coccoliths dominated, while non-calcifying cells were readily abundant in MCT and HCT. We also observed cells with residues of coccoliths (Fig. 5b), indicating hampered calcification.

4 Discussion

4.1 Effect of CO_2 on aggregate sinking velocity

Our study showed that exposure to different CO_2 concentrations during cell growth can affect properties and therewith sinking velocities of aggregates of *E. huxleyi*. Increasing

CO_2 concentration reduced the PIC content and increased the POC content of cell suspension and aggregates as well. Sinking velocities were highest for LCT aggregates, while MCT aggregates sank about half as fast as LCT aggregates. Sinking velocity was comparatively slow for HCT, although these aggregates reached the greatest sizes in this experiment.

Sinking velocity of aggregates in the ocean is highly variable, ranging from a few to several hundred meters per day, depending on the location, currents, composition, and other factors (Fowler and Knauer, 1986; Ploug et al., 2008; Fischer and Karakaş, 2009). Unlike natural marine snow, aggregates in this experiment were made of *E. huxleyi* cells solely. Engel et al. (2009b) determined sinking velocities of aggregates of calcified and non-calcified *E. huxleyi*, and observed rates of 1.0 to 2.5 cm s^{-1} for ~0.1 cm aggregates derived from calcified cells, and a wider range, from 0.1 to 2.0 cm s^{-1}, for the ~0.1 to 1.0 cm aggregates from non-calcified cells. During this study, we determined a similar range of sinking velocity and sizes for LCT and HCT aggregates that contained only marginal amounts of calcite. Thereby, settling velocities of HCT aggregates were well within the range of natural aggregates (Ploug et al., 2008; Fischer and Karakaş, 2009).

Porosities of all aggregates of this experiment were, although in the upper range, well comparable to porosities observed for field aggregates. Reports of marine snow porosities range from of >95 to 99.9% (Alldredge and Gotschalk, 1988; Ploug et al., 2008). Porosities of *E. huxleyi* aggregates, derived from a calcifying strain were reported to be in median 95.9% and for non-calcifying cells 99.6% (Engel et al., 2009b).

During this study, size of aggregates differed between treatments, although non-consistently. HCT aggregates reached the largest dimensions, being even larger than the LCT aggregates. A significant correlation between size (ESD, cm) and sinking velocity (cm s^{-1}) was determined for aggregates of the LCT treatment only, yielding $y=3.75x^{0.7}$ (Fig. 2). MCT aggregates showed a weak increase of settling velocity with size, while no change was observed for sinking rates of HCT aggregates over the whole size range (Fig. 2). For comparison, earlier studies yielded $y=1.94x^{0.89}$ for

a non-calcifying strain of *E. huxleyi* and $y=3.5x^{0.33}$ for a calcifying strain (Engel et al., 2009b). The sinking velocity ($m\,d^{-1}$) of natural marine snow that was investigated by Alldrege and Gotschalk (1988) increased with particle diameter (mm) according to $y=50x^{0.26}$.

While chemical composition was more similar for aggregates of MCT and HCT, excess density and porosity were more similar for LCT and MCT when regarding all aggregates. This can be explained by the strong influence of size on porosity and excess density in aggregates. It has been observed earlier that the porosity of aggregates decreases with size in a non-linear function (Alldredge and Gotschalk, 1988). Hence, in order to evaluate the effect on CO_2 induced changes in chemical composition on aggregate properties, we needed to compare aggregates at similar sizes. For mass of aggregates, this clearly revealed a decrease when going from LCT to HCT treatment (Fig. 4). Thereby, mass of MCT was more similar to HCT than to LCT, which agrees well with the chemical composition changes, e.g. the PIC density fraction. We also observed a higher variability in mass for HCT aggregates, than for MCT or LCT. From SEM pictures, we noticed that some cells in HCT still had residues of coccoliths, while others were fully non-calcified. Assuming that PIC was mainly responsible for differences in aggregate mass, this may indicate that PIC content of aggregates was quite variable, depending on the remaining amount of calcite. This may thus explain the observed higher variability in aggregate mass in HCT.

It is interesting to note, that differences in mass of aggregates were much larger than expected from differences in densities of calcite versus organic components, and can only be explained assuming that calcite also influences the porosity of aggregates. This was indeed observed in a similar type of study, comparing aggregates made of either calcified or non-calcified *E. huxleyi* (Engel et al., 2009b). We therefore conclude that even small changes in biogenic mineral content of aggregates may have large effects on aggregate properties and hence on sinking velocity.

Our study thus supports the hypothesis that biogenic ballast, a primarily biogenic calcite, significantly affects the deep export of organic matter (Ittekot and Haake, 1990;

Armstrong et al., 2002; Klaas and Archer, 2002).

4.2 Effect of CO_2 on the chemical composition of aggregates and the optical assessment of aggregates by SEM

Biogeochemical analyses showed that the ratio of particulate inorganic carbon (PIC) to particulate organic carbon (POC) was lowest for the HCT aggregate fraction compared to MCT and LCT. The decrease of PIC/POC ratios in *E. huxlyei* due to increased CO_2 conditions has been observed earlier and was attributed to more pronounced POC production combined with a decrease in calcification rate (Riebesell et al., 2000; Zondervan et al., 2001, 2002). However, other studies found no effect of CO_2 on PIC/POC ratios (Sciandra et al., 2003).

PIC/POC ratios in these earlier studies ranged from 0.77 to 1.02 at CO_2 concentrations of 27 to 6 µmol L^{-1} and were thus much higher than ratios observed during our experiment. However, PIC/POC ratios for LCT were comparable to those observed during an *E. huxleyi* bloom that was followed in the course of an outdoor mesocosm experiment (i.e. 0.23–0.29; Engel et al., 2005). A large range of PIC/POC ratios was also determined for the cells of the coccolithophore *Gephyrocapsa oceanica*, ranging from 0.17 to 1.18 at CO_2 concentration between 33.7 to 5.7 µmol L^{-1} (Zondervan et al., 2001). In the field, phytoplankton blooms often harbour a mixture of different taxa, including *E. huxleyi*. Here, PIC/POC ratios smaller than 0.25 are not uncommon (Marañón and González, 1997).

We therefore assume that all scenario aggregates of this experiment may be representative for aggregates occurring after coccolithophore blooms, if no other ballasting particles than biogenic $CaCO_3$ are present.

The largest TPV was observed for aggregates in the HCT. Despite that, the DW of the HCT aggregate fraction was the lowest of the three CO_2 treatments. The elevated TPV in MCT and HCT was likely due to an enhanced POC production. The Redfield ratio for carbon to nitrogen of 6.6 was only observed for cell suspensions at the very beginning of the incubation (data not shown). The POC to PON ratio of the aggregate

fraction at T21 was well above the Redfied-Ratio for the LCT, and even 3-fold higher for MCT and HCT. It has been suggested that C to N ratios increase in response to rising CO_2 concentration in a future ocean, mainly due to an enhanced organic carbon production (Hein and Sand-Jensen, 1997; Engel, 2002; Engel et al., 2005; Delille et al., 2005; Riebesell et al., 2007). During this experiment an increased production of POC combined with a decrease in mineral ballast in form of $CaCO_3$. Applied to the future ocean, consequences of our findings on total export of POC are difficult to estimate. One possible future scenario would be that reduced sinking velocities lead to a more shallow export, with potentially higher subsequent turn-over of organic matter and increased oxygen demand in the twilight zone. In this case, the profile of organic carbon distribution may move solely towards higher POC amounts in the upper and middle ocean, whereas the deep ocean may stay unaffected. This scenario could result in a weakening of deep export, and hence in the efficiency of the biological pump, provided that no other ballasting material, e.g. of terrigenous origin (e.g. dust), will be available to balance the loss.

It has been proposed that vertical transport of aggregates is triggered by POC and not by lithogenic ballast (Berelson, 2002; Passow, 2004). The presence of lithogenic material could even reduce the transport of aggregated material to depth (Hamm, 2002; Passow and De La Rocha, 2006). Following these arguments, a higher amount of POC in the sea could favour the aggregation of other mineral particulates already present in the water column, which may especially be the case in coastal areas and those receiving a high rate of atmospheric deposition.

During this study, the large amount of aggregates in the HCT contained also the largest amount of associated bacteria. This result is conclusive, since the HCT aggregates provided the largest area for bacterial attachment due to their large size and porosity, and also a higher amount of POC. It was shown earlier that degradation was enhanced in aggregates of non-calcified compared to calcified cells (Engel et al., 2009a). If a loss of calcite reduces the protection of organic matter from bacterial degradation, HCT aggregates may be subject to enhanced degradation. Hence, if

representative for the future ocean, a CO_2 induced loss in aggregate calcite may also affect organic matter export due to its effect on the lability of organic components.

SEM pictures of the aggregates supported the findings of the biogeochemical analysis: whereas the SEM pictures of LCT aggregates readily showed coccoliths, very few coccoliths could be identified in HCT aggregates. Moreover, the SEM pictures of HCT aggregates showed a large number of "naked". It has been reported earlier that changes in coccoliths morphology and reduced calcification of coccolithophores occur in response to high CO_2 treatments (Riebesell et al., 2000; Zondervan et al., 2001; Langer et al., 2006). Little is known, however, with respect to complete decalcification of coccolithophores under increased CO_2 concentrations. Though, there are reports of coccolithophores bearing only a few or one coccolith in dense natural blooms or senescent cultures (Paasche, 2002). It can't be excluded that the "naked" cells are haploid, non-calcifying S-cells, since the identification of S-cells and the distinction between both is difficult (Klaveness, 1972; Paasche, 2002). In a recent study it was shown that viral infection induced lysis in calcified diploid *E. huxleyi* cells, and the transition to the non-calcified haploid phase of *E. huxleyi* (Frada et al., 2008). If the loss of calcification in cells of our experiment were due to viral infection, this may indicate that HCT cells are more susceptible to viral infection.

5 Conclusions

Ocean acidification may induce changes in the composition and quality of biogenic particles that impact the formation, as well as the sinking and degradation rate of aggregates. As a consequence, the efficiency of deep export may be reduced in the future ocean, and the shallow remineralisation of organic matter enhanced. Thus, our study provides an example of how the biological pump may transmit the signal of anthropogenic perturbations from the surface into the ocean's interior.

Acknowledgements. This study was supported by the Helmholtz Association (contract no. HZ-NG-102) and by the Belgian Federal Science Policy Office in the framework of the PEACE

project (contract no. SD/CS/03A/B). Thanks go M. Lunau for his support with the flow cytometer measurements, to N. Händel for nutrient measurements, and to S. Koch for helping setting up the CO_2 aeration system.

References

Alldredge, A. and Gotschalk, C.: In situ settling behaviour of marine snow, Limnol. Oceanogr., 33(3), 339–351, 1988.

Armstrong, R. A., Lee, C., Hedges, J. I., Honjo, S., and Wakeham, S. G.: A new, mechanistic model for organic carbon flux in the ocean based on the quantitative association of POC with ballast minerals, Deep-Sea Res. Pt. II, 49, 219–236, 2002.

Berelson, W. A.: Particle settling rates increase with depth in the ocean, Deep-Sea Res. Pt. II, 237–251, 2001.

Brewer, P. G., Bradshaw, A. L., and Williams, R. T.: Measurements of total carbon dioxide and alkalinity in the North Atlantic in 1981. In: The Changing Carbon Cycle, edited by: Trabalka, J. R. and Reichle, D. E., Springer, New York, 349–370, 1986.

Delille, B., Harlay, J., Zondervan, I., Jacquet, S., Chou, L., Wollast, R., Bellerby, R. G. J., Frankignoulle, M., Borges, A. V., Riebesell, U., and Gattuso, J.-P.: Response of primary production and calcification to changes of pCO_2 during experimental blooms of the coccolithophorid *Emiliania huxleyi*, Global Biogeochem. Cy., 19, GB2023, doi:10.1029/2004GB002318, 2005.

Dietrich, G., Kalle, K., Krauss, W., and Siedler, G.: Allgemeine Meereskunde: Eine Einführung in die Ozeanographie, Gebrüder Borntraeger, Berlin, Stuttgart, 593 pp., 1975.

Engel, A. and Schartau, M.: Influence of transparent exopolymer particles (TEP) on sinking velocity of *Nitzschia closterium* aggregates, Mar. Ecol. Prog. Ser., 182, 69–76, 1999.

Engel, A., Goldthwait, S., Passow, U., and Alldredge, A.: Temporal decoupling of carbon and nitrogen dynamics in a mesocosm diatom bloom. Limnol. Oceanogr., 47(3), 753–761, 2002.

Engel, A., Zondervan, I., Aerts, K., Beaufort, L., Benthien, A., Chou, L., Delille, B., Gattuso, J.-P., Harley, J., Heemann, C., Hoffmann, L., Jacquet, S., Nejstgaard, J., Pizay, M.-D., Rochelle-Newall, E., Schneider, U., Terbrüggen, A., and Riebesell, U.: Testing the direct effect of CO_2 concentration on a bloom of the coccolithophorid *Emiliania huxleyi* in mesocosm experiments, Limnol. Oceanogr., 50(2), 493–507, 2005.

Engel, A., Abramson, L., Szlosek, J., Liu, Z., Stewart, G., Hirschberg, D., and Lee, C.: Investigating the effect of ballasting by $CaCO_3$ in *Emiliania huxleyi*, II: Decomposition of particulate organic matter, Deep-Sea Res. Pt. II, 56(18), 1408–1419, doi:10.1016/j.dsr2.2008.028, 2009a.

Engel, A., Szlosek, J., Abramson, L., Liu, Z., and Lee, C.: Investigating the effect of ballasting by $CaCO_3$ in *Emiliania huxleyi*: I. Formation, settling velocities and physical properties of aggregates, Deep-Sea Res. Pt. II, 56(18), 1397–1407, doi:10.1016/j.dsr2.2008.027, 2009b.

Fischer, G. and Karakaş, G.: Sinking rates and ballast composition of particles in the Atlantic Ocean: implications for the organic carbon fluxes to the deep ocean, Biogeosciences, 6, 85–102, 2009, http://www.biogeosciences.net/6/85/2009/.

Fowler, S. W. and Knauer, G. A.: Role of large particles in the transport of elements and organic compounds through the oceanic water column, Prog. Oceanogr., 16, 147–194, 1986.

Frada, M., Probert, I., Allen, M. J., Wilson, W. H., and de Vargas, C.: The "Cheshire Cat" escape strategy of the coccolithophore *Emiliania huxleyi* in response to viral infection, PNAS, 105(41), 15944–15949, 2008.

Francois, R., Honjo, S., Krishfield, R., and Manganini, S.: Factors controlling the flux of organic carbon to the bathypelagic zone of the ocean, Global Biogeochem. Cy., 16(4), 1087, doi:10.1029/2001GB001722, 2002.

Gasol, J. M. and and del Giorgio, P. A.: Using flow cytometry for counting natural planktonic bacteria and understanding the structure of planktonic bacterial communities, Sci. Mar., 64(2), 197–224, 2000.

Gran, G.: Determination of the equivalence point in potentiometric titrations, part II, Analyst, 77, 661–671, 1952.

Grasshoff, K., Kremling, K., and Ehrhardt, M. with contributions by Anderson, L. G.: Methods of Seawater Analysis, 3rd edn., Wiley-VCH, Weinheim, 1999.

Guillard, R. R. and Ryther, J. H.: Studies of marine planktonic diatoms, I. *Cyclotella nana* Hustedt and *Detonula confervacea* (Cleve) Gran, Can. J. Mikrobiol. 8, 229–239, 1962.

Hamm, C. E.: Interactive aggregation and sedimentation of diatoms and clay-sized lithogenic material, Limnol. Oceanogr., 47(6), 1790–1795, 2002.

Hein, M. and Sand-Jensen, K.: CO_2 increases oceanic primary production, Nature, 388, 526–527, 1997.

Holligan, P. M., Viollier, M., Harbour, D. S., Camus, P., and Champagne-Philippe, M.: Satellite

and ship studies of coccolithophore production along a continental shelf edge, Nature, 304, 339–342, 1983.
Honjo, S., Manganini, S. J., and Cole, J. J.: Sedimentation of biogenic matter in the deep ocean, Deep-Sea Res. A, 29(5), 609–625, 1982.
Iglesias-Rodriguez, M. D., Halloran, P. R., Rickaby, R. E. M., Hall, I. R., Colmenero-Hidalgo, E., Gittins, J. R., Green, D. R. H., Tyrell, T., Gibbs, S. J., von Dassow, P., Rehm, E., Armbrust, E. V., and Boessenkool, K. P.: Phytoplankton in a High-CO_2 World, Science, 320, 336–340, 2008.
Ittekkot, V. and Haake, B.: The terrestrial link in the removal of organic carbon in the sea. In: Facets of Modern Biogeochemistry, edited by: Ittekkot, V., Kempe, S., Michaelis, M., Spitzy, A., Springer, Berlin, 318–325, 1990.
Klaas, C. and Archer, D. E.: Association of sinking organic matter with various types of mineral ballast in the deep sea: Implications for the rain ratio, Global Biogeochem. Cy., 16(4), 1116, doi:10.1029/2001GB001765, 2002.
Klaveness, D.: *Coccolithus huxleyi* (Lohm.) Kamptn, II. The flagellate cell, aberrant cell types, vegetative propagation and life cycles, Br. Phycol. J., 309–318, 1972.
Kleypas, J. A., Feely, R. A., Fabry, V. J., Langdon, C., Sabine, C. L., and Robbins, L. L.: Impacts of ocean acidification on coral reefs and other marine calcifiers: A guide for future research, report of a workshop held 18–20 April 2005, St. Petersburg, FL, sponsored by NSF, NOAA and the US Geological Survey, 88 pp., 2006.
Langer G., Geisen, M., Baumann, K.-H., Kläs, J., Riebesell, U., Thoms, S., and Young, J. R.: Species-specific responses of calcifying algae to changing seawater carbonate chemistry, Geochem. Geophys. Geosy., 7(9), Q09006, doi:10.1029/2005GC001227, 2006.
Langer, G., Nehrke, G., Probert, I., Ly, J., and Ziveri, P.: Strain-specific responses of *Emiliania huxleyi* to changing seawater carbonate chemistry, Biogesciences Discuss., 6, 4361–4383, 2009.
Lewis, E. and Wallace, D. W. R.: Program developed for CO_2 system calculations. ORNL/CDIAC-105, Carbon dioxide information analysis centre, Oak Ridge National Laboratory, US Department of Energy, Oak Ridge, Tennessee, 1998.
Marañón, E. and González, N.: Primary production, calcification and macromolecular synthesis in a bloom of the coccolithophore *Emiliania huxleyi* in the North Sea, Mar. Ecol. Prog. Ser., 157, 61–77, 1997.
Paasche, E.: A review of the coccolithophorid *Emiliania huxleyi* (Prymnesiophyceae), with par-

ticular reference to growth, coccolith formation, and calcification-photosynthesis interactions, Phycologia, 40(6), 503–529, 2002.
Passow, U.: Switching perspectives: Do mineral fluxes determine particulate organic carbon fluxes or vice versa? Geochem. Geophys. Geosy., 5(4), Q04002, doi:10.1029/2003GC000670, 2004.
Passow, U. and De La Rocha, C. L.: Accumulation of mineral ballast on organic aggregates, Global Biogechem. Cy., 20, GB1013, doi:10.1029/2005GB002579, 2006.
Ploug, H. and Iversen, M. H.; Ballast, sinking velocity, and apparent diffusivity within marine snow and zooplankton fecal pellets: Implications for substrate turnover by attached bacteria, Limnol. Oceanogr., 53(5), 1878–1886, 2008.
Raitos, D. E., Lavender, S. J., Pradhan, Y., Tyrell, T., Reid, P. C, and Edwards, M.: Coccolithophore bloom size variation in response to the regional environment of the subarctic North Atlantic, Limnol. Oceanogr., 51(5), 2122–2130, 2006.
Redfield, A. C., Ketchum, B. M., and Richards, F. A.: The influence of organism on the composition of sea-water. In: The Sea, edited by: Hill, M. N., John Wiley and Sons, New York, 26–77, 1963.
Riebesell, U., Zondervan, I., Rost, B., Tortell, P. D., Zeebe, R. E., and Morel, F. M. M.: Reduced calcification of marine plankton in response to increased atmospheric CO_2, Nature, 407, 364–367, 2000.
Riebesell, U., Schulz, K. G., Bellerby, R. G. J., Botros, M., Fritsche, P., Meyerhöfer, M., Neill, C., Nondal, G., Oschlies, A., Wohlers, J., and Zöllner, E.: Enhanced biological carbon consumption in a high CO_2 ocean, Nature, 450, 545–548, 2007.
Robertson, J. E., Robinson, C., Turner, D. R., Holligan, P., Watson, A. J., Boyd, P., Fernandez, E., and Finch, M.: The impact of a coccolithophore bloom on oceanic carbon uptake in the northeast Atlantic during summer 1991. Deep-Sea Res. Pt. I., 41(2), 297–314, 1994.
Rost, B., Riebesell, U., and Burkhardt, S.: Carbon acquisition of bloom-forming marine phytoplankton, Limnol. Oceanogr., 48(1), 55–67, 2003.
Sabine, C. L., Feely, R. A., Gruber, N., Key, R. M., Lee, K., Bullister, J. L., Wanninkhof, R., Wong, C. S., Wallace, D. W. R., Tilbrook, B., Millero, F. J., Peng, T.-H., Kozyr, A., Ono, T., and Rios, A. F.: The oceanic sink for anthropogenic CO_2, Science, 305, 367–371, 2004.
Sciandra, A., Harlay, J., Lefèvre, D., Lemée, R., Rimmelin, P., Denis, M., and Gattuso, J.-P.: Response of coccolithophorid *Emiliania huxleyi* to elevated partial pressure of CO_2 under nitrogen limitation, Mar. Ecol.-Prog. Ser., 261, 111–122, 2003.

Smayda, T. J.: The suspension and sinking of phytoplankton in the sea, Oceanogr. Mar. Biol. Ann. Rev., 8, 353–414, 1970.

Tooby, P. F., Wick, G. L., and Isaacs, J. D.: The Motion of a small sphere in a rotating velocity field: a possible mechanism for suspending particles in turbulence, J. Geophys. Res., 82(15), 2096–2100, 1977.

Van der Wal, P., Kempers, R. S., and Veldhuis, M. J. W.: Production and downward flux of organic matter and calcite in a North Sea bloom of the coccolithophore *Emiliania huxleyi*, Mar. Ecol. Prog.-Ser., 126, 247–265, 1995.

Zondervan, I., Zeebe, R. E., Rost, B., and Riebesell, U.: Decreasing marine biogenic calcification: A negative feedback on rising atmospheric pCO_2, Global Biogeochem. Cy., 15(2), 507–516, 2001.

Zondervan, I., Rost, B., and Riebesell, U.: Effect of CO_2 concentration on the PIC/POC ratio in the coccolithophore *Emiliania huxleyi* grown under light-limiting conditions and different day lengths, J. Exp. Mar. Biol. Ecol., 272, 55–70, 2002.

Table 1. Sampling plan.

Timepoint	DW/bacteria	cellcounts/TPV	nutrients	PIC/POC/TPC/PON	pH	TA	SEM
Start aeration							
day 0 (T0)	–	×	×	×	×	×	×
day 6 (T6)	–	×	–	×	×	×	×
Start aggregation							
day 14 (T14)	×	×	×	×	×	×	×
End aggregation							
day 21(T21)	×	×	×	×	×	×	×

Table 2. Chemical and biological composition of the cell suspension before the roller table experiment was started (T14).

Parameter	Unit	LCT	MCT	HCT
TPV	$mm^3\,L^{-1}$	82.8	112	91.0
TPC	$mg\,L^{-1}$	29.9±1.38	47.3±0.465	40.7±2.02
POC	$mg\,L^{-1}$	19.0±1.42	33.8±0.978	31.9±1.53
PIC	$mg\,L^{-1}$	10.9±2.59	13.5±1.04	9.42±4.00
PON	$mg\,L^{-1}$	2.13±0.08	1.90±0.082	1.86±0.114
DW	$mg\,L^{-1}$	778±64.5	908±48.5	750±110
Bacteria	L^{-1}	7.27×10^8	3.20×10^9	1.95×10^9
PIC/POC	mol/mol	0.579±0.177	0.399±0.041	0.298±0.140
TPC/PON	mol/mol	17.5±0.223	31.2±1.03	27.5±0.334
POC/PON	mol/mol	11.2±1.23	22.3±1.14	21.3±2.65
$\Omega_{calcite}$	–	6.5	2.8	1.7

Table 3. Slurry volumes of each tank that were isolated after the roller table experiment.

	Slurryvolume [ml]		
Tank vol.	LCT	MCT	HCT
10 L	77.1	69.8	117.9
4.5 L a	21.4	86.7	97.5
4.5 L b	21.6	14.9	96.0
Total	**120.1**	**171.4**	**311.4**

Table 4. Results per litre tank volume of the chemical and biological analysis of the aggregate fraction (AGG) and enrichment factor (f) in aggregates after the roller tank experiment (T21).

Parameter	Unit	LCT AGG	f	MCT AGG	f	HCT AGG	f
TPV	$mm^3\,L^{-1}$	5.77±0.921	10	10.2±3.55	8	19.5±6.33	12
TPC	$mg\,L^{-1}$	1.37±0.353	11	3.19±0.804	13	5.83±1.45	12
POC	$mg\,L^{-1}$	1.22±0.328	16	3.01±0.507	16	5.81±1.41	13
PIC	$mg\,L^{-1}$	0.150±0.100	2.8	0.215±0.303	4.0	0.130±0.095	2.0
PON	$mg\,L^{-1}$	0.134±0.048	16	0.147±0.035	13	0.311±0.095	11
DW	$mg\,L^{-1}$	39.9±15.8	7.2	37.4±15.2	6.5	38.2±16.5	2.0
Bacteria	$10^8\,L^{-1}$	2.77±1.22	56	3.45±1.76	38	5.51±3.03	28
DW/TPV	mg/mm^3	6.69±3.83	0.66	3.09±0.104	0.85	1.81±0.334	0.16
PIC/TPV	mg/mm^3	0.026±0.018	0.30	0.017±0.021	0.69	0.007±0.004	0.18
POC/TPV	mg/mm^3	0.209±0.022	1.6	0.310±0.066	2.7	0.307±0.051	1.1
PIC/POC	mol/mol	0.127±0.096	0.19	0.063±0.084	0.53	0.023±0.017	0.17
POC/PON	mol/mol	11.8±1.84	0.98	25.9±2.11	1.2	24.0±4.01	1.2
POC/TPC	mol/mol	0.890±0.082	1.5	0.957±0.084	1.2	0.997±0.023	1.1
$\Omega_{calcite}$	–	4.8±0.9	–	1.8±0.1	–	1.4±0.1	–

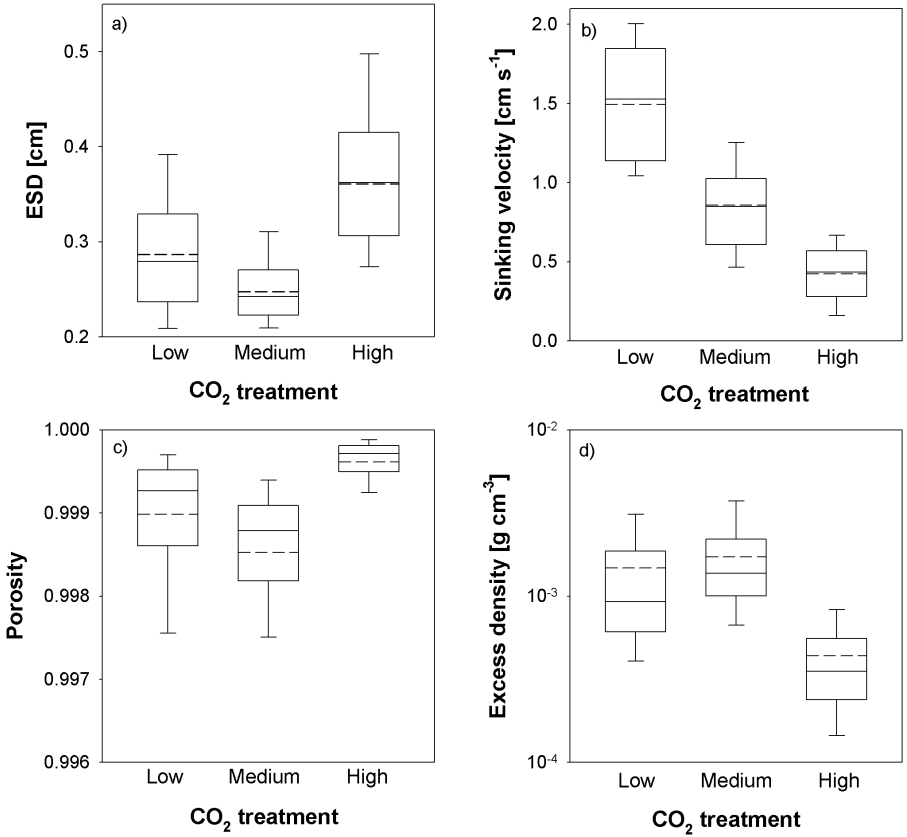

Fig. 1. **(a)** equivalent spherical diameter (ESD), **(b)** sinking velocity, **(c)** porosity and **(d)** excess density of aggregates in the three CO_2 treatments during the roller table experiment. Pooled data of four days (T14–T18) during the incubation (180: n=71, 380: n=63, 750: n=65). Median=solid line, mean=dashed line. Length of the box expresses the spread of the data set (25–75%), error bars (10–90%).

BGD
6, 9817–9848, 2009

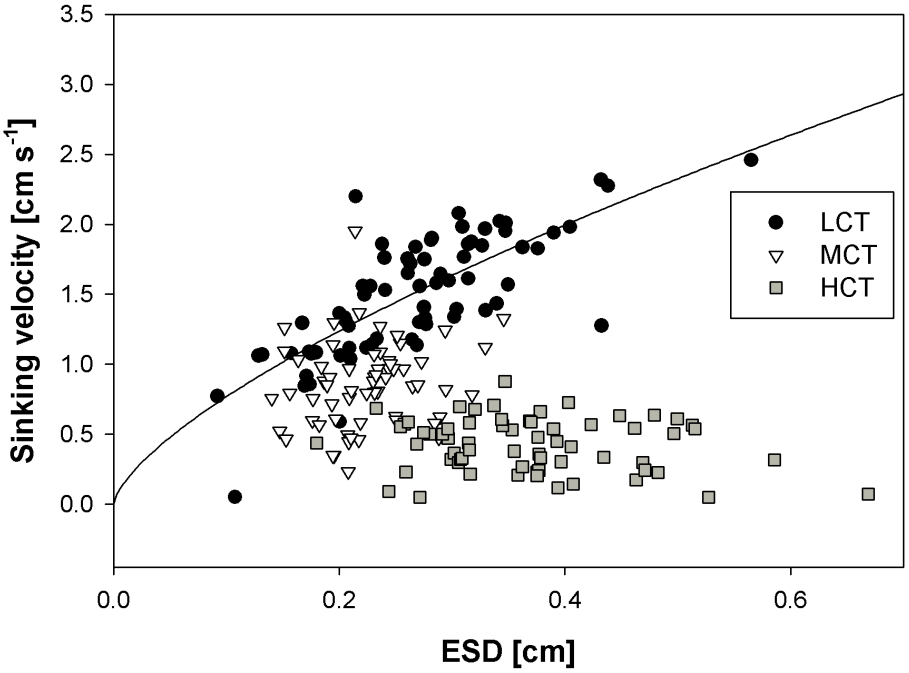

Fig. 2. Sinking velocity ($cm\,s^{-1}$) in relation to the equivalent spherical diameter (ESD, cm) of the aggregates in the three CO_2 treatments during the roller table experiment. The curve fit to the LCT (filled dots) is $y=3.75x^{0.7}$ ($r^2=0.58$). (For *n* see Fig. 1).

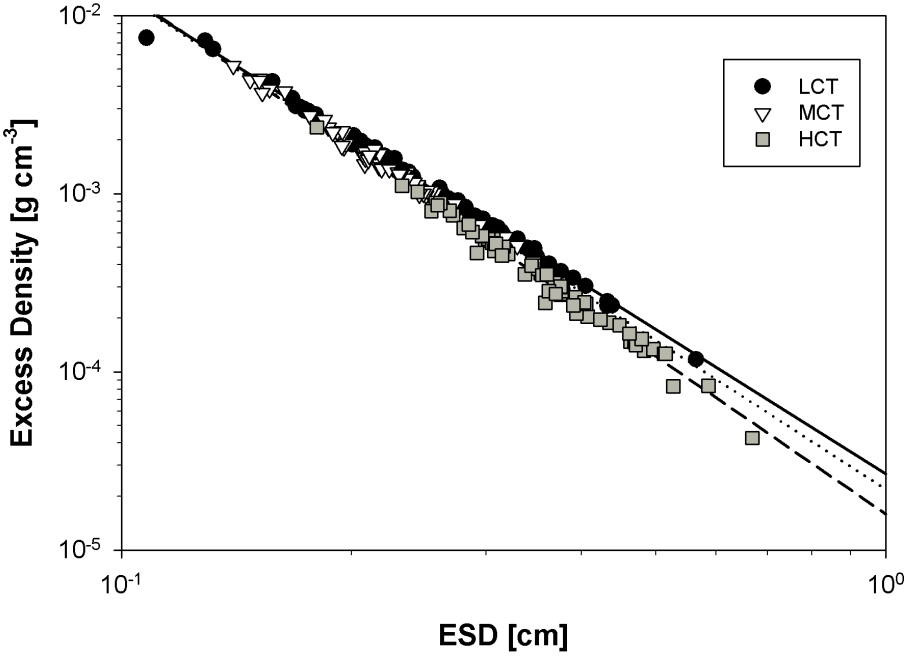

Fig. 3. Excess density (g cm^{-3}) in relation to the equivalent spherical diameter (ESD, cm) of the aggregates in the three CO_2 treatments during the roller table experiment. (For *n* see Fig. 1). The excess density of aggregates was related to the ESD with the power decay function for LCT: $y=3\times10^{-5}x^{-2.69}$ ($r^2=0.99$) (solid line), for MCT: $y=2\cdot10^{-5}x^{-2.78}$ ($r^2=0.99$) (dotted line) and for HCT: $y=2\cdot10^{-5}x^{-2.94}$ ($r^2=0.99$) (dashed line).

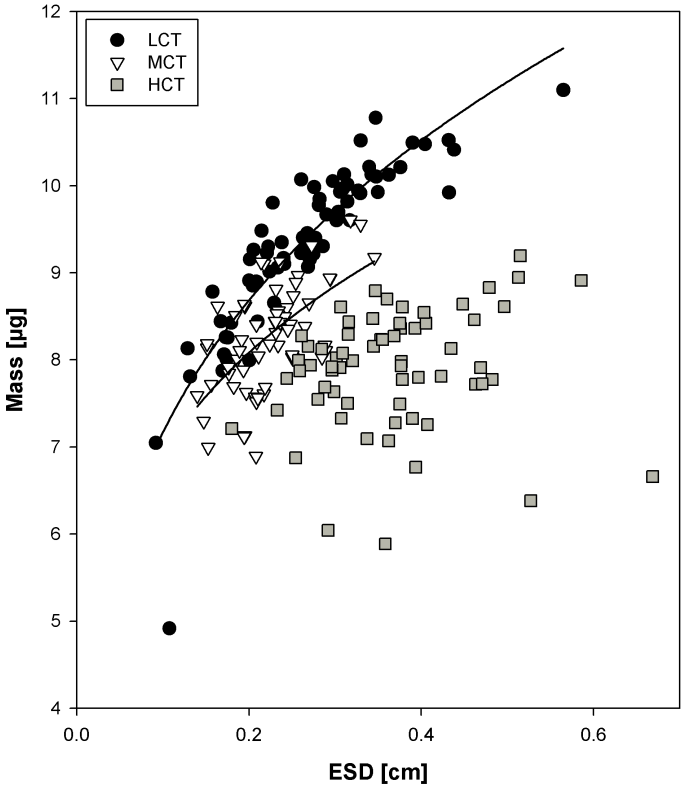

Fig. 4. Mass (µg) of aggregates in relation to their equivalent spherical diameter (ESD, cm) in the three CO_2 treatments during the roller table experiments. (For *n* see Fig. 1). For LCT, mass of aggregates was related to the ESD with the power function $y=13.6x^{0.28}$ ($r^2=0.79$). The relationship of mass for the MCT aggregates was less pronounced with $y=11.6x^{0.22}$ ($r^2=0.37$).

BGD
6, 9817–9848, 2009

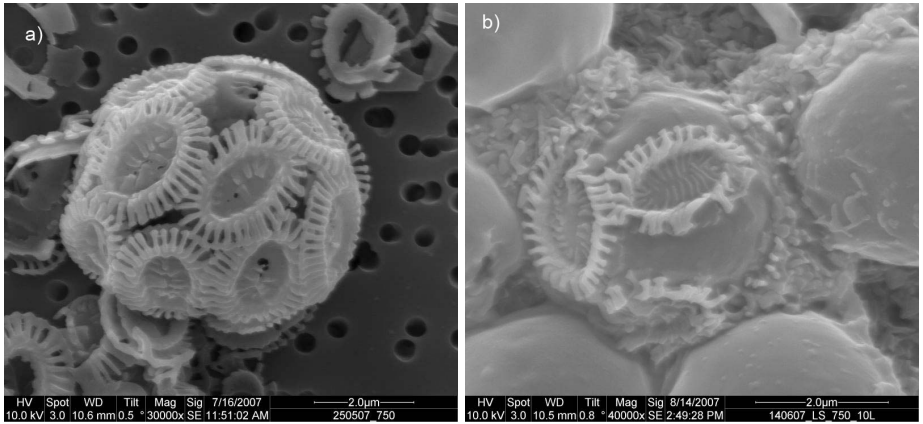

Fig. 5. SEM pictures of a calcified *E. huxleyi* from the beginning of the CO_2-inoculation (T0) (left) and from the HCT of the suspension at the end of the aggregation experiment (T21) (right). This "missing link" indicates a defragmentation or detachment of coccoliths.